Frequency-domain Adaptive Parametric Model Order Reduction Method for Oscillatory Stability Analysis on Multi-converter-fed Systems

Xun Jiang, *Student Member*, *IEEE*, Meiqin Mao, Liuchen Chang, *Senior Member*, *IEEE*, Bao Xie, Haijiao Wang, *Member*, *IEEE*, and Nikos D. Hatziargyriou, *Fellow*, *IEEE*

***Abstract*—The oscillatory stability analysis of multi-converter-fed systems (MCFSs) with modest computational resources needs a precise parametric reduced-order impedance model (PROIM). However, the traditional Krylov subspace based parametric model order reduction (KS-PMOR) method has difficulty in building precise PROIM for MCFSs. This is because the factors related to the errors of PROIM are complicated and coupled. To fill this gap, the factors associated with the accuracy of the KS-PMOR method are estimated by defining three indicators: the convergence error, cumulative error, and rank of projection matrix. Using the three indicators, a frequency-domain adaptive parametric model order reduction (FDA-PMOR) method is developed to form the precise PROIM of MCFSs for the accurate and fast oscillatory stability analysis. The accuracy of the obtained PROIM using the proposed FDA-PMOR method and its efficiency in actual oscillatory stability analysis are validated by three MCFSs with different scales, i. e., a small-scale MCFS with four paralleled converter-based renewable energy generators (CREGs), a real-time simulation-based MCFS with eighteen paralleled CREGs, and a larger MCFS with ninety paralleled CREGs.**

***Index Terms*—Multi-converter-fed system (MCFS), oscillatory stability analysis, frequency-domain adaptive parametric model order reduction (FDA-PMOR), parametric reduced-order impedance.**

NOMENCLATURE

A. Indices and Sets

$\mathbb{C}$	Set of complex numbers
d, q	Indices for d and q axes
h	Index of positions of frequency window
i	Index of frequency interpolation points
j	Index of parameter interpolation points
k	Index of parameter subspaces
$s_{\mathrm{a},h}$	Set of extra-added frequency interpolation points in frequency window at the h^{th} position
s_{s}, s_{o}	Sets of frequency interpolation points in rank-sensitive and rank-insensitive sub-frequency bands
$\mathbb{S}_k$	The k^{th} parameter subspace of multi-converter-fed system (MCFS)

B. Parameters

Ω	Frequency band of model order reduction
$\Omega_{\mathrm{sc},h}$	Frequency window at the h^{th} position
ω_1, ω_2	The minimum and maximum frequencies of Ω
ω_{p}	Bandwidth of low-pass filer in phase-locked loop (PLL)
f_{s}	Switching frequency of converter for converter-based renewable energy generators (CREGs)
Δg	Number of extra-added frequency interpolation points within $\Omega_{\mathrm{sc},h}$
I_{d0}	d-axis output current of each CREG at steady-state setpoints
k_{ps}	Number of parameter subspaces
K_{c}	Active damping factor of current controller
K_{ip}, K_{ii}	Proportion and integration factors of current controller
K_{pllp}, K_{plli}	Proportion and integration factors of PLL
L_{g}, L_{m}, R_{d}, C	Grid-side inductance, converter-side inductance, damping resistance, and filter capacitance of output filter for CREG
N_{c}	Total number of paralleled CREGs in MCFS

Manuscript received: April 11, 2024; revised: July 18, 2024; accepted: October 29, 2024. Date of CrossCheck: October 29, 2024. Date of online publication: November 27, 2024.

This work was supported by Open Fund of State Key Laboratory of Operation and Control of Renewable Energy & Storage Systems (China Electric Power Research Institute) (No. NYB51202201695), National Natural Science Foundation of China (No. 51677050), and 111 Project (No. BP0719039).

This article is distributed under the terms of the Creative Commons Attribution 4.0 International License (http://creativecommons.org/licenses/by/4.0/).

X. Jiang, M. Mao (corresponding author), and B. Xie are with the Research Center for Photovoltaic System Engineering of Ministry of Education, Hefei University of Technology, Hefei 230009, China (e-mail: jaysonxun@163. com; mmqmail@163.com; x.bao@hfut.edu.cn).

L. Chang is with the University of New Brunswick, Fredericton, New Brunswick E3B 5A3, Canada (e-mail: lchang@unb.ca).

H. Wang is with the State Key Laboratory of Operation and Control of Renewable Energy & Storage Systems (China Electric Power Research Institute), Beijing 100192, China (e-mail: wanghaijiao@epri.sgcc.com.cn).

N. D. Hatziargyriou is with the National Technical University of Athens, Athens 15780, Greece (e-mail: nh@power.ece.ntua.gr).

DOI: 10.35833/MPCE.2024.000390

N_{f}, N_{p}	Numbers of frequency and parameter interpolation points
R_{rec}, C_{rec}	Buffer resistance and compensation capacitance of reactive power compensator
S_{f}	State space of full-order model for MCFS
Th_{c}, Th_{ce}	Threshold values of convergence and cumulative errors
Z_{grid}	Grid line impedance

C. Miscellaneous Information

λ	Varying parameter of CREG
ω	Synchronization phase of PLL
Ω_{s}, Ω_{is}	Rank-sensitive and rank-insensitive sub-frequency bands
$\boldsymbol{A}_{\mathrm{C},dq}$, $\boldsymbol{B}_{\mathrm{C},dq}$, $\boldsymbol{C}_{\mathrm{C},dq}$	State, input, and output matrices of CREG in dq-axis
$\boldsymbol{A}_{\mathrm{M},q}$, $\boldsymbol{B}_{\mathrm{M},q}$, $\boldsymbol{C}_{\mathrm{M},q}$	State, input, and output matrices of MCFS in q-axis
$\boldsymbol{A}_{\mathrm{r}}$, $\boldsymbol{B}_{\mathrm{r}}$, $\boldsymbol{C}_{\mathrm{r}}$	Reduced-order state, input, and matrices of MCFS
$\boldsymbol{B}_{\mathrm{e}}(s_i)$, $\boldsymbol{X}_{\mathrm{e}}(s_i)$	Cumulative errors of $\boldsymbol{B}_{\mathrm{M},q}(\lambda_j)$ and $\boldsymbol{X}(s_i)$ at s_i
$\boldsymbol{E}_{\mathrm{c}}(s_i)$	Convergence error of $\boldsymbol{X}(s_i)$ at s_i
E_{frob}	Frobenius norm of errors
i_q	Output current of MCFS in q-axis
$i_{\mathrm{g},dq,i}$	Output current of CREG in dq-axis
$i_{\mathrm{ref},dq}$	Current reference of CREG in dq-axis
$\boldsymbol{I}_q$, $\boldsymbol{I}_{\mathrm{r}}$	Identity matrices with sizes of $n \times n$ and $r \times r$
K_{r}	Krylov subspace
L	Impedance return ratio
$L_{\mathrm{r},h}$	Rank sensitive of $\Omega_{\mathrm{sc},h}$
L_{f}	Impedance return ratio based on full-order impedance model
$L_{\mathrm{KS\text{-}PMOR}}$	Impedance return ratio based on traditional Krylov subspace based parametric model order reduction (KS-PMOR) method
$L_{\mathrm{FDA\text{-}PMOR}}$	Impedance return ratio based on the proposed frequency-domain adaptive parametric model order reduction (FDA-PMOR) method
M_{cond}	Condition number of $\boldsymbol{M}_i(\lambda_j)$
n	Size of full-order model
$n_{\mathrm{k},i}$	Order of moments at s_i
N_{fs}, N_{fo}	Numbers of frequency interpolation points in Ω_{s} and Ω_{is}
r	Size of reduced-order model
$\Delta R_{\mathrm{T},h}$	Variation of rank of projection matrix $\boldsymbol{T}_{\mathrm{p}}$ at the h^{th} position
$\boldsymbol{T}_{\mathrm{p}}$	Projection matrix
$u_{\mathrm{g},q,i}$	Voltage at point of common coupling (PCC) of CREG in q-axis
$u_{\mathrm{Mg},q}$	Voltage at PCC of MCFS in q-axis
V_{dc}	DC input voltage of CREG
$\boldsymbol{x}_{dq}$, $\boldsymbol{u}_{dq}$, $\boldsymbol{y}_{dq}$	State, input, and output vectors of CREG in dq-axis
$\boldsymbol{x}_{\mathrm{M},q}$	Full-order state vector of MCFS
$\boldsymbol{x}_{\mathrm{r}}$	Reduced-order state vector of MCFS
$\boldsymbol{X}(s_i)$	State vector at s_i
$X_{\mathrm{e,frob}}$	Frobenius norm of $\boldsymbol{X}_{\mathrm{e}}$
$\boldsymbol{X}_N(s_i)$	$\boldsymbol{X}(s_i)$ obtained with N iterations
Z_{f}	Full-order impedance model of MCFS
$Z_{\mathrm{MCFS}}(s)$, $Z_{\mathrm{eg}}(s)$	Equivalent impedances of large-scale MCFS and external grid
Z_{r}	Parametric reduced-order impedance model of MCFS

I. Introduction

In future power systems, the increased renewable energy sources will be integrated into the grids. These renewable energy sources are generally interfaced with power electronic converters, which form various multi-converter-fed systems (MCFSs). The extensive application of MCFSs brings new challenges to the stable operation of power systems. Particularly, MCFSs with numerous parallel converter-based renewable energy generators (CREGs) may lead to unstable oscillations over a wide frequency range [1]. These small-signal oscillatory stability problems are caused by the complicated interaction between different MCFSs and the power system, and may be triggered at various operation points of the grid-tied MCFS. Thus, for variable MCFS in the constantly evolving power system, it is difficult to guarantee the stable operation of the system at all operation points by a one-time and offline stability assessment at the planning stage [2]. The real-time (or near real-time) analysis of the oscillatory stability at the operation stage of MCFSs [3]-[5] becomes essential, in order to monitor the potential oscillatory risk and prevent upcoming oscillations. However, the full-order models of MCFSs with a cluster of CREGs have extremely high dimension, making the oscillatory stability analysis a huge computational burden [6]. Precise reduced-order models of MCFSs are urgently required to enable the real-time (or near real-time) oscillatory stability analysis of MCFSs with low computational cost [5], [7].

The dominant mode preserved (DMP) methods are proposed for the model order reduction of synchronous machines decades ago [8]. They have also been extended to reduce the model order of MCFSs in recent years. Using the DMP methods, the dominant modes of MCFSs are retained [9], [10] or reconstructed [11], [12] by the singular perturbation method, Jordan continued fraction expansion method, etc. However, the dominant modes of MCFSs usually change with variable system parameter sets, such as the operation points and pre-set controller parameters. Thus, the DMP methods cannot provide suitable reduced-order models because they cannot preserve system parameters during the model order reduction.

The weighted coherency (WCO) method, inspired by the coherency equivalence method in traditional power systems, can preserve the system parameters during the model order reduction. Using this method, the model size of MCFS is reduced by aggregating different CREGs into a single [13], [14] or multiple [15], [16] equivalent CREGs. The system parameters are preserved by establishing the relationship be-

tween the parameters of individual and equivalent CREGs. However, the WCO method simplifies some specific units in the MCFS, such as output filters and control units of CREGs. This may lead to significant errors during the model order reduction and make it unsuitable for the accurate small-signal oscillatory stability studies [6], [17].

In addition, the above methods only have high accuracy for model order reduction on some specific time scales (mostly slow time scales), and thus are inadequate to accurately estimate the oscillatory stability of MCFS over a wide frequency range. In the last few years, the impedance models have been proposed to describe the wide-band frequency-domain characteristics of MCFSs at the point of common coupling (PCC). The impedance models have been widely applied to analyze the practical oscillatory stability issues of various MCFSs owing to their universal applicability, intuitive stability criteria, and ability to access the oscillatory stability margins [18]. However, the full-order impedance model of a practical MCFS with numerous CREGs needs to be described by thousands or even tens of thousands of equations. The oscillatory stability analysis of MCFSs using full-order impedance models is also challenging [6].

In recent literature, the data-driven impedance (DDI) methods have been proposed to build the parametric reduced-order impedance model (PROIM) of MCFS. The obtained PROIM can preserve some specific parameter accesses of the original full-order model and retain its corresponding parameter-dependent characteristics. For example, by incorporating artificial intelligence methods into the traditional frequency scanning method, the PROIM can be built without knowing the detailed structure and parameters of MCFS [19]. However, the PROIM needs to be trained using an extremely large amount of high-quality frequency response data with different system parameters. For the actual grid-tied MCFS, the high-quality frequency response data are usually difficult to collect, and it is challenging to guarantee the wide-band accuracy of the obtained PROIM at all possible operation points [6], [20]. These hinder the development of DDI methods for MCFSs.

Recently, the non-parametric projection-based model order reduction (NPJMOR) methods have been proposed to reduce the size of full-order impedance models for MCFSs [21], [22]. In the NPJMOR methods, the model order reduction is realized by projecting the full-order impedance model into a reduced state space using a projection matrix. The NPJMOR method can guarantee a high-accuracy model order reduction at fixed system parameters without specific unit simplification or additional data requirements. Thus, it can be used as a generalized method for various MCFSs. However, the non-parameter preserved reduced-order impedance model built by the NPJMOR method can only be used for the oscillatory stability analysis of MCFS at specific operation points rather than for varying operation points.

So far, several parametric model order reduction methods have been reported for different fields. For example, the sparse low-rank Choleski factor alternate direction implicit based balanced truncation (SLRCF-ADI-BT) method has been proposed to build the parametric reduced-order model for the small-signal electromechanical stability analysis of large-scale power systems [23], [24]. In this method, the specific parameter-dependent equipment is segmented into a subsystem of the large-scale power system. The parametric model order reduction is realized by completely retaining the segmented subsystem. However, for MCFS, all the CREGs are parameter-dependent, and the subsystem segmentation is difficult to realize in large-scale power systems [23]. Reference [25] presents the Krylov subspace based parametric model order reduction (KS-PMOR) method to build the parametric reduced-order model for the large-scale circuit design of operational amplifiers. This method can be used to build the parametric reduced-order model without complex matrix calculations (e.g., solving the Lyapunov equation in the balanced truncation method), which makes it more suitable for the model order reduction of systems with extremely high order, like the MCFS [26]. However, the KS-PMOR method derives the projection matrix suitable for full system parameter sets by interpolation [27]. The accuracy of the obtained reduced-order model strongly depends on the adopted interpolation strategies [26]. To the best of the author's knowledge, there are no general interpolation strategies for the application of KS-PMOR method in different fields. The error mechanism and general interpolation optimizing method need to be carefully investigated before it is applied to build the precise PROIM of MCFS.

The individual features of the various model order reduction methods discussed above are compared in Table I in terms of parameter preserving ability (PPA), necessity of specific unit reduction/retention (NSUR), the high demand of frequency response data (HDFRD), and capability for oscillatory stability analysis (COSA). It can be observed that all methods present insufficiencies in different properties that restrict their efficiency for oscillatory stability analysis. The KS-PMOR method performs better in the three properties, but it still needs to be further improved to build the precise PROIM and apply it to oscillatory stability analysis. As far as the authors know, the parametric model order reduction method for building wide-band accurate PROIM across all system parameter sets for MCFS has not yet been reported in the current literature.

TABLE I
COMPARISON OF DIFFERENT MODEL ORDER REDUCTION METHODS

Method	PPA	NSUR	HDFRD	COSA
DMP	No	No	No	No
WCO	Yes	Yes	No	No
DDI	Yes	No	Yes	No
NPJMOR	No	No	No	No
SLRCF-ADI-BT	Yes	Yes	No	No
KS-PMOR	Yes	No	No	Pending

To fill this gap, this paper proposes a frequency-domain adaptive parametric model order reduction (FDA-PMOR) method to form the PROIM of MCFS suitable for a wide-band frequency domain over the full parameter range.

The main contributions of this paper are as follows.

1) The error mechanism of the traditional KS-PMOR method is quantitatively evaluated by defining three indicators, i.e., the convergence error, cumulative error, and rank of projection matrix.

2) The FDA-PMOR method is proposed to build the PROIMs of MCFSs in the *dq*-frame. This method can adaptively optimize the parameters and frequency interpolation strategies based on the three indicators. The obtained PROIM can characterize system features over the full parameter range with wider-band accuracy and a smaller model size.

3) The feasibility of the proposed FDA-PMOR method and its effect on actual oscillatory stability analysis are evaluated using three MCFSs with different scales, i.e., a small-scale MCFS with four paralleled CREGs, a real-time simulation-based MCFS with eighteen paralleled CREGs, and a larger MCFS with ninety paralleled CREGs.

The rest of this paper is organized as follows. Section II presents the full-order impedance model of a typical MCFS. In Section III, the FDA-PMOR method is proposed based on the error mechanism analysis of the traditional KS-PMOR method. The proposed FDA-PMOR method is verified by three MCFSs with different scales in Section IV followed with conclusions in Section V.

II. Full-order Impedance Model of A Typical MCFS

The topology of a typical MCFS is shown in Fig. 1. Multiple CREGs are connected in parallel and integrated to the external grid at the same PCC. Different renewable energy generator technologies can provide the DC-side power supply of each CREG.

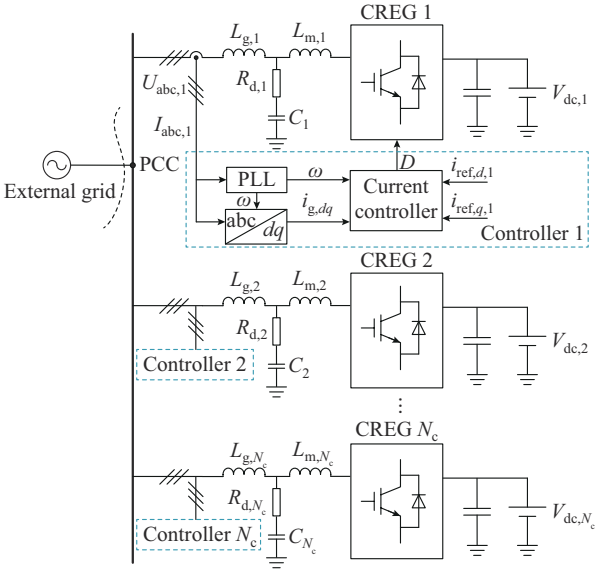

Fig. 1. Topology of a typical MCFS.

The small-signal model of a single CREG with varying parameters λ can be expressed as [28]:

$$\begin{cases} \dot{\boldsymbol{x}}_{dq} = \boldsymbol{A}_{\mathrm{C},dq}(\lambda)\boldsymbol{x}_{dq} + \boldsymbol{B}_{\mathrm{C},dq}(\lambda)\boldsymbol{u}_{dq} \\ \boldsymbol{y}_{dq} = \boldsymbol{C}_{\mathrm{C},dq}(\lambda)\boldsymbol{x}_{dq} \end{cases} \tag{1}$$

The full-order small-signal model of MCFS with N_c paralleled CREGs cannot be obtained by simply scaling the full-order small-signal model of the individual CREGs. In this paper, the coupling term among the CREGs is neglected by assuming that there is no unstable interaction among individual CREGs [29]. Thereby, the full-order small-signal model of MCFS with N_c paralleled CREGs can be represented by:

$$\begin{cases} \begin{bmatrix} \dot{\boldsymbol{x}}_{dq,1} \\ \dot{\boldsymbol{x}}_{dq,2} \\ \vdots \\ \dot{\boldsymbol{x}}_{dq,N_c} \end{bmatrix} = \begin{bmatrix} \boldsymbol{A}_{\mathrm{C},dq,1}(\lambda) & 0 & \dots & 0 \\ 0 & \boldsymbol{A}_{\mathrm{C},dq,2}(\lambda) & \dots & 0 \\ \vdots & \vdots & & \vdots \\ 0 & 0 & \dots & \boldsymbol{A}_{\mathrm{C},dq,N_c}(\lambda) \end{bmatrix} \begin{bmatrix} \boldsymbol{x}_{dq,1} \\ \boldsymbol{x}_{dq,2} \\ \vdots \\ \boldsymbol{x}_{dq,N_c} \end{bmatrix} + \\ \qquad \begin{bmatrix} \boldsymbol{B}_{\mathrm{C},dq,1}(\lambda) \\ \boldsymbol{B}_{\mathrm{C},dq,2}(\lambda) \\ \vdots \\ \boldsymbol{B}_{\mathrm{C},dq,N_c}(\lambda) \end{bmatrix} \begin{bmatrix} \boldsymbol{u}_{dq,1} \\ \boldsymbol{u}_{dq,2} \\ \vdots \\ \boldsymbol{u}_{dq,N_c} \end{bmatrix} \\ \boldsymbol{y}_{dq} = [\boldsymbol{C}_{\mathrm{C},dq,1}(\lambda) \quad \boldsymbol{C}_{\mathrm{C},dq,2}(\lambda) \quad \dots \quad \boldsymbol{C}_{\mathrm{C},dq,N_c}(\lambda)] \cdot \\ \qquad [\boldsymbol{x}_{dq,1} \quad \boldsymbol{x}_{dq,2} \quad \dots \quad \boldsymbol{x}_{dq,N_c}]^{\mathrm{T}} \end{cases} \tag{2}$$

This full-order small-signal model of MCFS has an extremely high order. Although the state matrix of MCFS is a diagonal matrix composed of $\boldsymbol{A}_{\mathrm{C},dq}$, it is challenging to solve such a full-order model in real time (or near realtime) with acceptable computational costs.

In this paper, the *q*-axis full-order small-signal model of MCFS (from input $\Delta u_{\mathrm{Mg},q}$ to output Δi_q) containing the majority of the dynamic characteristics is used to evaluate the proposed FDA-PMOR method.

$$\begin{cases} \dot{\boldsymbol{x}}_{\mathrm{M},q} = \boldsymbol{A}_{\mathrm{M},q}(\lambda)\boldsymbol{x}_{\mathrm{M},q} + \boldsymbol{B}_{\mathrm{M},q}(\lambda)\Delta u_{\mathrm{Mg},q} \\ \Delta i_q = \boldsymbol{C}_{\mathrm{M},q}(\lambda)\boldsymbol{x}_{\mathrm{M},q} \end{cases} \tag{3}$$

where $\boldsymbol{A}_{\mathrm{M},q}(\lambda) = \mathrm{diag}(\boldsymbol{A}_{\mathrm{C},q,1}(\lambda), \boldsymbol{A}_{\mathrm{C},q,2}(\lambda), \dots, \boldsymbol{A}_{\mathrm{C},q,N_c}(\lambda))$; $\boldsymbol{B}_{\mathrm{M},q}(\lambda) = [\boldsymbol{B}_{\mathrm{C},q,1}(\lambda), \boldsymbol{B}_{\mathrm{C},q,2}(\lambda), \dots, \boldsymbol{B}_{\mathrm{C},q,N_c}(\lambda)]^{\mathrm{T}}$; $\boldsymbol{C}_{\mathrm{M},q}(\lambda) = [\boldsymbol{C}_{\mathrm{C},q,1}(\lambda), \boldsymbol{C}_{\mathrm{C},q,2}(\lambda), \dots, \boldsymbol{C}_{\mathrm{C},q,N_c}(\lambda)]$; $\boldsymbol{x}_{\mathrm{M},q} = [\boldsymbol{x}_{q,1}, \boldsymbol{x}_{q,2}, \dots, \boldsymbol{x}_{q,N_c}]^{\mathrm{T}}$; and $\Delta i_q = \Delta i_{\mathrm{g},q,1} + \Delta i_{\mathrm{g},q,2} + \dots + \Delta i_{\mathrm{g},q,N_c}$.

Converting the *q*-axis full-order small-signal model in (3) to the frequency domain, the *q*-axis impedance model $Z_{\mathrm{f}}(s,\lambda)$ of MCFS can be represented as (4). The frequency-domain characteristics of $Z_{\mathrm{f}}(s,\lambda)$ are highly related to the varying parameters λ [30].

$$\begin{cases} \Delta i_q(s) = Z_{\mathrm{f}}^{-1}(s,\lambda)\Delta u_{\mathrm{Mg},q}(s) \\ Z_{\mathrm{f}}(s,\lambda) = \dfrac{1}{\boldsymbol{C}_{\mathrm{M},q}(\lambda)(s\boldsymbol{I}_q - \boldsymbol{A}_{\mathrm{M},q}(\lambda))^{-1}\boldsymbol{B}_{\mathrm{M},q}(\lambda)} \end{cases} \tag{4}$$

Due to the high dimensionality of matrices $\boldsymbol{A}_{\mathrm{M},q}(\lambda)$, $\boldsymbol{B}_{\mathrm{M},q}(\lambda)$, and $\boldsymbol{C}_{\mathrm{M},q}(\lambda)$, the oscillatory stability analysis using $Z_{\mathrm{f}}(s,\lambda)$ requires very high computational resources as well as the detailed structure and parameters of MCFS. MCFS vendors can usually easily access the specific control structure and parameters. In this case, the generation of full-order impedance models is straightforward. Thus, this paper focuses on how to address the model order reduction of $Z_{\mathrm{f}}(s,\lambda)$.

III. Proposed FDA-PMOR Method

In this section, the error mechanism of KS-PMOR method is analyzed to identify the main factors affecting the accura-

cy of the reduced-order model. Subsequently, the FDA-PMOR method is proposed to build the high-precision PROIM of MCFS for oscillatory stability analysis.

A. KS-PMOR Method

Using the KS-PMOR method, the full-order small-signal model of MCFS with varying parameters in (3) can be projected to a low-dimensional state space via the projection matrix $\boldsymbol{T}_{\mathrm{p}} \in \mathbb{C}^{r\times n}(r \ll n)$, yielding the parametric reduced-order small-signal model of MCFS as:

$$\begin{cases} \dot{\boldsymbol{x}}_{\mathrm{r}} = \boldsymbol{A}_{\mathrm{r}}(\lambda)\boldsymbol{x}_{\mathrm{r}} + \boldsymbol{B}_{\mathrm{r}}(\lambda)\Delta u_{\mathrm{Mg},q} \\ \Delta i_q = \boldsymbol{C}_{\mathrm{r}}(\lambda)\boldsymbol{x}_{\mathrm{r}} \end{cases} \tag{5}$$

where $\boldsymbol{A}_{\mathrm{r}}(\lambda) = \boldsymbol{T}_{\mathrm{p}}\boldsymbol{A}_{\mathrm{M},q}(\lambda)\boldsymbol{T}_{\mathrm{p}}^{\mathrm{T}}$; $\boldsymbol{B}_{\mathrm{r}}(\lambda) = \boldsymbol{T}_{\mathrm{p}}\boldsymbol{B}_{\mathrm{M},q}(\lambda)$; $\boldsymbol{C}_{\mathrm{r}}(\lambda) = \boldsymbol{C}_{\mathrm{M},q}(\lambda)\boldsymbol{T}_{\mathrm{p}}^{\mathrm{T}}$; and $\boldsymbol{x}_{\mathrm{r}} = \boldsymbol{T}_{\mathrm{p}}\boldsymbol{x}_{\mathrm{M},q}$. The PROIM of MCFS can be derived by performing the Laplace transform on (5):

$$Z_{\mathrm{r}}(s,\lambda) = \frac{1}{\boldsymbol{C}_{\mathrm{r}}(\lambda)(s\boldsymbol{I}_{\mathrm{r}} - \boldsymbol{A}_{\mathrm{r}}(\lambda))^{-1}\boldsymbol{B}_{\mathrm{r}}(\lambda)} \tag{6}$$

Here, the projection matrix $\boldsymbol{T}_{\mathrm{p}}$ plays a key role in obtaining the low-order and high-precision PROIM. It can be spanned by mutually orthogonal state vectors $\boldsymbol{X}(s_i)$ at multi-frequency interpolation points via the KS-PMOR method [31]:

$$\boldsymbol{T}_{\mathrm{p}} \supseteq span\{\boldsymbol{X}(s_i)\} \quad s_i \in \Omega, i = 1, 2, ..., N_{\mathrm{f}} \tag{7}$$

To ensure the accuracy, the obtained reduced-order small-signal model in (5) should have the same moments in the first $n_{\mathrm{k},i}$ orders at each frequency interpolation point (FIP) s_i as the full-order small-signal model in (3). Thus, $\boldsymbol{X}(s_i)$ needs to satisfy (8) to fall into the Krylov subspace $K_{\mathrm{r}}(\boldsymbol{X}_i; \boldsymbol{Y}_i)$ as in (9).

$$(s_i\boldsymbol{I}_q - \boldsymbol{A}_{\mathrm{M},q}(\lambda))\boldsymbol{X}(s_i) = \boldsymbol{B}_{\mathrm{M},q}(\lambda) \tag{8}$$

$$\begin{cases} \boldsymbol{X}(s_i) \in K_{\mathrm{r}}(\boldsymbol{X}_i; \boldsymbol{Y}_i) \\ K_{\mathrm{r}}(\boldsymbol{X}_i; \boldsymbol{Y}_i) = span\{\boldsymbol{X}_i, \boldsymbol{Y}_i\boldsymbol{X}_i, \boldsymbol{Y}_i^2\boldsymbol{X}_i, \ldots, \boldsymbol{Y}_i^{n_{\mathrm{k},i}-1}\boldsymbol{X}_i\} \end{cases} \tag{9}$$

where $\boldsymbol{Y}_i = (s_i\boldsymbol{I}_q - \boldsymbol{A}_{\mathrm{M},q}(\lambda))^{-1}$; and $\boldsymbol{X}_i = (s_i\boldsymbol{I}_q - \boldsymbol{A}_{\mathrm{M},q}(\lambda))^{-1}\boldsymbol{B}_{\mathrm{M},q}(\lambda)$.

For the full-order small-signal model of MCFS with varying parameters, there exists no explicit solution to $\boldsymbol{X}(s_i)$ that satisfies (8) over the full parameter range. To deal with this problem, the recursive least square method has been introduced to convert the explicit solving problem of $\boldsymbol{X}(s_i)$ into the optimization problem [25]:

$$\begin{cases} \min\limits_{\boldsymbol{X}(s_i)} \sum\limits_{j=1}^{N_{\mathrm{p}}} \left\| (s_i\boldsymbol{I}_q - \boldsymbol{A}_{\mathrm{M},q}(\lambda_j))\boldsymbol{X}(s_i) - \boldsymbol{B}_{\mathrm{M},q}(\lambda_j) \right\|_{\mathrm{F}}^2 \\ \text{s.t. } \boldsymbol{X}(s_i) \in \mathbb{C}^{n\times 1} \end{cases} \tag{10}$$

where $\|\cdot\|_{\mathrm{F}}$ represents the Frobenius norm. The optimization objective is to solve $\boldsymbol{X}(s_i)$ with the minimum error at all parameter interpolation points. In this paper, the variation range of λ_j is fixed. Thus, according to the standard least square method, (10) can be easily reformulated to matrix calculation as:

$$\boldsymbol{X}(s_i) = \left(\sum_{j=1}^{N_{\mathrm{p}}} \boldsymbol{M}_i^{\mathrm{H}}(\lambda_j)\boldsymbol{M}_i(\lambda_j) \right)^{-1} \sum_{j=1}^{N_{\mathrm{p}}} \boldsymbol{M}_i^{\mathrm{H}}(\lambda_j)\boldsymbol{B}_{\mathrm{M},q}(\lambda_j) \tag{11}$$

where the superscript H represents the conjugate transpose; and $\boldsymbol{M}_i(\lambda_j) = s_i\boldsymbol{I}_q - \boldsymbol{A}_{\mathrm{M},q}(\lambda_j)$.

In the KS-PMOR method, $\boldsymbol{T}_{\mathrm{p}}$ can be obtained with different parameter interpolation sets of λ_j and different frequency interpolation sets of s_i. Different sets of λ_j and s_i will affect the accuracy of model order reduction. Thus, the selection of λ_j and s_i is very important for maintaining a wide-band frequency-domain accuracy of the obtained PROIM of MCFS. However, in the current literature, it has not quantitively identified the influence of different λ_j and s_i on the errors of the reduced-order model using the KS-PMOR method.

B. Analysis of Error Mechanism of KS-PMOR Method

In this subsection, the error mechanism of KS-PMOR method is analyzed using a small-scale MCFS with four paralleled CREGs as an example. The topology of the small-scale MCFS is shown in Fig. 1, and the detailed parameters of four parallel CREGs are presented in Supplementary Material A Table SAI. During the error mechanism analysis, the output current I_{d0} of each CREG at steady-state setpoints is set as the preserved parameter, and the frequency band of model order reduction is set as 0-2000 Hz.

1) Error Mechanism of Solving State Vectors

In the KS-PMOR method, one of the most important procedures is to solve the state vector $\boldsymbol{X}(s_i)$ at each FIP.

According to (11), the matrix inversion can be well-posed in the ideal cases, where $\boldsymbol{M}_i(\lambda_j)$ is nonsingular, and $\boldsymbol{M}_i^{\mathrm{H}}(\lambda_j)\boldsymbol{M}_i(\lambda_j)$ is positive definite. The optimization for $\boldsymbol{X}(s_i)$ can converge rapidly, and the accurate $\boldsymbol{X}(s_i)$ for the full parameter range can be obtained with a small number of iterations.

Nevertheless, due to the large differences in the magnitudes of MCFS parameters, the state matrix $\boldsymbol{A}_{\mathrm{M},q}(\lambda)$ of MCFS can be ill-conditioned with a high condition number. For instance, the control parameters of CREG are usually tens of orders larger than those of passive components in output filter of CREG. These factors will make $\boldsymbol{M}_i(\lambda_j)$ nearly singular, rendering the inversion of $\boldsymbol{M}_i^{\mathrm{H}}(\lambda_j)\boldsymbol{M}_i(\lambda_j)$ ill-posed and leading to errors in the optimization process of $\boldsymbol{X}(s_i)$. In this paper, the parameters of MCFS have already been rescaled based on the per-unit rules of power system. However, because of the restriction of the remaining characteristics, the parameters of MCFS cannot be scaled freely to completely eliminate the ill-condition of $\boldsymbol{A}_{\mathrm{M},q}(\lambda)$.

During the optimization process of (10), the error of $\boldsymbol{X}(s_i)$ can be expressed as [32]:

$$\begin{cases} \boldsymbol{B}_{\mathrm{e}}(s_i) = \sum\limits_{j=1}^{N_{\mathrm{p}}} [(s_i\boldsymbol{I}_q - \boldsymbol{A}_{\mathrm{M},q}(\lambda_j))\boldsymbol{X}(s_i) - \boldsymbol{B}_{\mathrm{M},q}(\lambda_j)] \\ \boldsymbol{X}_{\mathrm{e}}(s_i) = \boldsymbol{B}_{\mathrm{e}}(s_i)M_{\mathrm{cond}} \end{cases} \tag{12}$$

The error $\boldsymbol{X}_{\mathrm{e}}(s_i)$ accumulates over the iterations, which is named the cumulative error of $\boldsymbol{X}(s_i)$. To intuitively evaluate the variation of $\boldsymbol{X}_{\mathrm{e}}(s_i)$ along with the iteration number, the Frobenius norm of $\boldsymbol{X}_{\mathrm{e}}(s_i)$ in (13) is utilized. $X_{\mathrm{e,frob}}(s_i)$ at each FIP with different numbers of parameter interpolation points is shown in Fig. 2, where horizontal axis adopts the Logarithmic coordinate.

$$X_{\mathrm{e,frob}}(s_i) = \left\| \boldsymbol{X}_{\mathrm{e}}(s_i) \right\|_{\mathrm{F}} \tag{13}$$

In Fig. 2, $X_{\text{e,frob}}$ increases as N_{p} increases, which is also the iteration number to solve $\boldsymbol{X}(s_i)$, especially for low-frequency bands. Moreover, according to (12), the high M_{cond} will enlarge the error of $\boldsymbol{X}(s_i)$, which makes the accuracy of $\boldsymbol{X}(s_i)$ more sensitive to N_{p}.

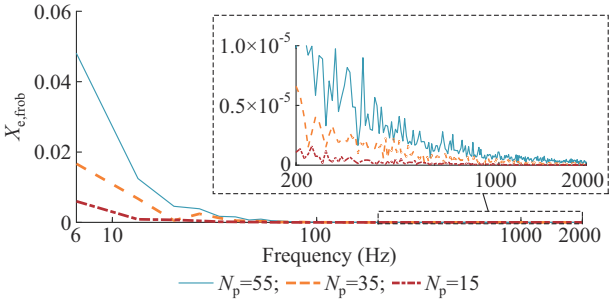

Fig. 2. Frobenius norm of $\boldsymbol{X}_{\text{e}}(s_i)$ at each FIP.

When solving $\boldsymbol{X}(s_i)$, the accuracy is also impacted by the convergence of the optimization progress. In this subsection, $E_{\text{c}}(s_i)$ is defined as the convergence error to quantitatively express the impact of the convergence of $\boldsymbol{X}(s_i)$ on the error of the model order reduction:

$$E_{\text{c}}(s_i)=\left|\boldsymbol{X}_N(s_i)-\boldsymbol{X}_{N-1}(s_i)\right| \tag{14}$$

where $|\cdot|$ denotes the mod operation of each element in the matrix. $\boldsymbol{X}(s_i)$ is considered to have reached convergence when $E_{\text{c}}(s_i)$ is less than the convergence threshold Th_{c}, which is set to be 0.01 in this paper.

Figure 3 shows the comparison of the minimum number of parameter interpolation points N_{p} for $\boldsymbol{X}(s_i)$ convergence with different ranges of I_{d0}. It can be observed that N_{p} increases as the range of I_{d0} becomes larger. This means that when I_{d0} varies over a larger range, more parameter interpolation points are needed to ensure the convergence of $\boldsymbol{X}(s_i)$. However, according to (12), more parameter interpolation points will introduce larger cumulative errors to $\boldsymbol{X}(s_i)$.

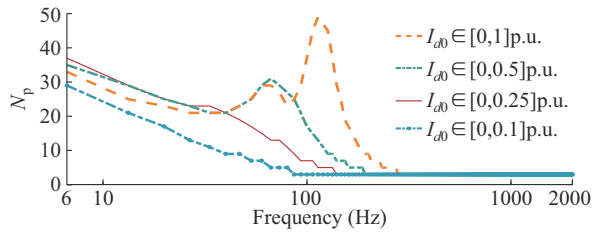

Fig. 3. Comparison of the minimum number of parameter interpolation points N_{p} for $\boldsymbol{X}(s_i)$ convergence with different ranges of I_{d0}.

2) Error Mechanism of Spanning Projection Matrix

Another essential process in the KS-PMOR method is the spanning of the projection matrix based on $\boldsymbol{X}(s_i)$ at each FIP.

In the KS-PMOR method, the Krylov subspace $K_{\text{r},i}$ at each FIP s_i should be able to form the state space of the full-order model of MCFS [31]. This means that any state of the full-order model of MCFS should be represented by the column vectors of the projection matrix as:

$$S_{\text{f}}=K_{\text{r},1}\cup K_{\text{r},2}\cup\ldots\cup K_{\text{r},i}=span\{\boldsymbol{X}(s_i)\}\quad s_i\in\Omega, i=1,2,...,N_{\text{f}} \tag{15}$$

According to (15), the column vectors of the projection matrix should be mutually orthogonal and contain the basis vectors of S_{f} as much as possible, so that the projection matrix can access more state space of the full-order model. Thus, the rank of projection matrix can be used to quantitatively evaluate the state space accessing of the projection matrix.

In this part, the Frobenius norm of model order reduction error $E_{\text{frob}}(s_i,\lambda)$ in (16) is used to analyze the relationship between the model order reduction error and the rank of projection matrix.

$$E_{\text{frob}}(s_i,\lambda)=\left\|Z_{\text{f}}(s_i,\lambda)-Z_{\text{r}}(s_i,\lambda)\right\|_{\text{F}} \tag{16}$$

The boxplot of the model order reduction error with different ranks of projection matrix $\boldsymbol{T}_{\text{p}}$ at different frequency points s_i is shown in Fig. 4. It can be observed that $E_{\text{frob}}(s_i,\lambda)$ of the obtained reduced-order impedance models will drop along with the increasing rank of projection matrix. This is because the projection matrix with a higher rank can access more state space in S_{f}. Thus, the reduced-order impedance model can have the accuracy in higher wide-band frequency domain.

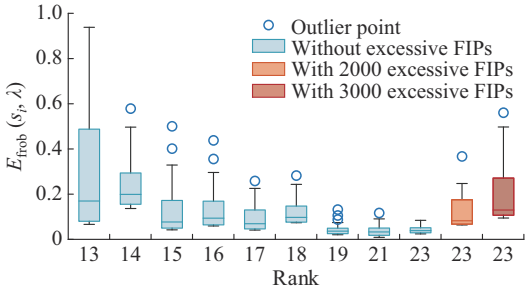

Fig. 4. Boxplot of model order reduction error with different ranks of projection matrix.

Before using projection matrix $\boldsymbol{T}_{\text{p}}$, the singular value decomposition (SVD) is usually utilized to obtain the first r basis vectors of $\boldsymbol{T}_{\text{p}}$ [33]. As mentioned above, the ill-posed $\boldsymbol{M}_i^{\text{H}}(\lambda_j)\boldsymbol{M}_i(\lambda_j)$ has a side effect on solving $\boldsymbol{X}(s_i)$ at each FIP. Maximizing the rank of $\boldsymbol{T}_{\text{p}}$ by excessive FIPs will introduce additional errors to $\boldsymbol{T}_{\text{p}}$, which may lead the SVD to extract the wrong basis vectors. These wrong basis vectors will influence the accuracy of model order reduction.

To validate the above discussions, the simulation results of two more cases are added to Fig. 4, where the rank of $\boldsymbol{T}_{\text{p}}$ is maximized by adding 2000 and 3000 excessive uniformly distributed FIPs. It can be observed that the excessive FIPs leads to significant errors during the model order reduction.

The following conclusions can be obtained.

1) Both the cumulative and convergence errors of $\boldsymbol{X}(s_i)$ will influence the accuracy of model order reduction. Therefore, it is vital to set a parameter interpolation strategy (optimizing N_{p} and k_{ps}) to converge $\boldsymbol{X}(s_i)$ without excessive cumulative errors.

2) The rank of projection matrix and the error of model order reduction are strongly correlated. A high-rank projection matrix can improve the accuracy of model order reduction. Consequently, the frequency interpolation strategy

should be optimized to maximize the rank of projection matrix with a minimum number of FIPs.

3) According to the quantitative analysis on the error mechanism of the KS-PROM method, the factors affecting the accuracy of model order reduction can be estimated by defining three indicators, i.e., the convergence error, cumulative error, and rank of projection matrix.

C. Proposed FDA-PMOR Method for MCFS

The FDA-PMOR method was initially proposed to form the PROIM of MCFS with high frequency-domain accuracy. Different from the traditional KS-PMOR method, the proposed FDA-PMOR method can optimize the parameters and frequency interpolation strategies adaptively based on the three indicators. The framework of the proposed FDA-PMOR method for MCFS is shown in Fig. 5. It consists of four stages discussed as follows.

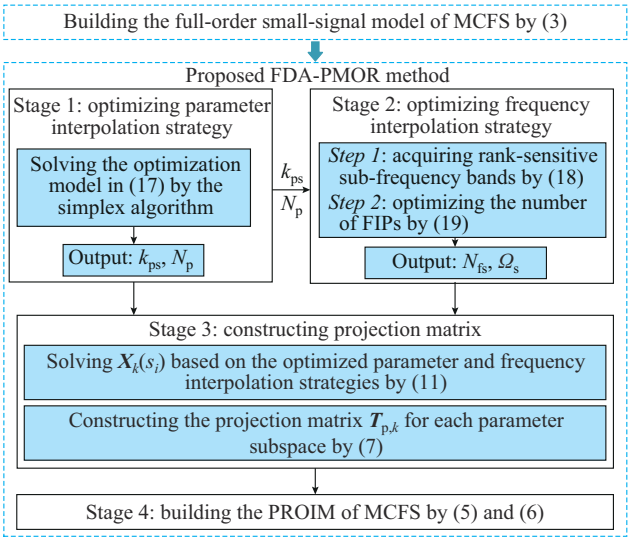

Fig. 5. Framework of proposed FDA-PMOR method for MCFS.

1) Stage 1: Optimizing Parameter Interpolation Strategy

The first stage of the proposed FDA-PMOR method is optimizing the parameter interpolation strategy. According to the error mechanism analysis, the solution process of $\boldsymbol{X}(s_i)$ needs to ensure the convergence of $\boldsymbol{X}(s_i)$ without excessive cumulative errors. Therefore, the cumulative and convergence errors of $\boldsymbol{X}(s_i)$ are introduced as constraints to (10), and we can obtain:

$$\begin{cases} \min\limits_{\boldsymbol{X}(s_i)} \sum\limits_{j=1}^{N_p} \left\| (s_i \boldsymbol{I}_q - \boldsymbol{A}_{\mathrm{M},q}(\lambda_{j,k}))\boldsymbol{X}(s_i) - \boldsymbol{B}_{\mathrm{M},q}(\lambda_{j,k}) \right\|_{\mathrm{F}}^2 \\ \text{s.t. } \boldsymbol{X}(s_i) \in \mathbb{C}^{n\times 1} \\ \quad 1 \le k \le k_{ps} \\ \quad \max(\boldsymbol{E}_c(s_i)) \le Th_c \\ \quad X_{e,frob}(s_i) < Th_{ce} \end{cases} \tag{17}$$

During the solution progress of (17), the parameter interpolation strategy (optimizing N_p and k_{ps}) ensures that the solution process of $\boldsymbol{X}(s_i)$ can meet the error constraints. Since the number of feasible solutions for N_p-k_{ps} combination is finite, the optimal solution of N_p and k_{ps} can be derived after a finite number of iterations by the simplex algorithm. Thus, the parameter interpolation strategy is optimized first.

2) Stage 2: Optimizing Frequency Interpolation Strategy

As illustrated in Section III-B, the high-rank projection matrix can improve the accuracy of model order reduction. Consequently, the frequency interpolation strategy is optimized for constructing the high-rank projection matrix in two steps, as shown in Fig. 6. At this stage, the rank-sensitive sub-frequency bands are first acquired by the frequency window scanning. Then, the number of FIPs in the rank-sensitive sub-frequency band are optimized to maximize the rank of projection matrix. The detailed steps are described as follows.

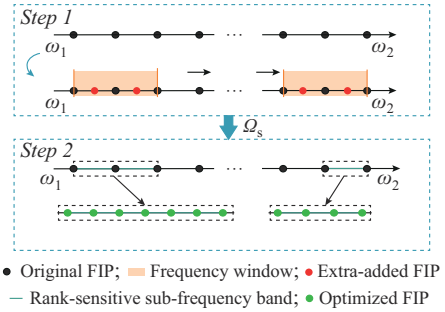

Fig. 6. Diagram of optimizing frequency interpolation strategy.

Step 1: the frequency band $\Omega=[\omega_1, \omega_2]$ of model order reduction is scanned by the frequency window $\Omega_{sc,h}$ ($h=1,2,3,\ldots$) from ω_1 to ω_2. In each $\Omega_{sc,h}$, the extra-added FIPs $s_{a,h}$ with the number of Δg are added, as shown in Fig. 6.

The projection matrix $\boldsymbol{T}_{p,h}$ is constructed based on s_o and $s_{a,h}$ using (7). In (7), $\boldsymbol{X}(s_i)$ ($s_i \in s_o \cup s_{a,h}$) is solved with the optimized parameter interpolation strategy obtained at Stage 1. The rank sensitivity of $\Omega_{sc,h}$ denoted as $L_{r,h}$ can be calculated by:

$$L_{r,h} = \frac{\Delta R_{T,h}}{\Delta g} \quad L_{r,h} \ge 0 \tag{18}$$

If $L_{r,h}>0$, it means that $\Omega_{sc,h}$ is rank-sensitive and the FIPs should be added to raise the rank of projection matrix. If $L_{r,h}=0$, the original FIPs in $\Omega_{sc,h}$ are sufficient to maximize the rank of projection matrix. Thus, by calculating $L_{r,h}$ in each $\Omega_{sc,h}$, the rank-sensitive sub-frequency bands Ω_s can be obtained.

Step 2: based on the obtained rank-sensitive sub-frequency bands Ω_s, the number of FIPs N_{fs} in Ω_s needs to be minimized to maximize the rank of projection matrix. Thus, the rank maximization of projection matrix is set as the objective function, and the optimization model of N_{fs} is formed as:

$$\begin{cases} \max rank(\boldsymbol{T}_p) = rank(span\{\boldsymbol{X}(s_s), \boldsymbol{X}(s_o)\}) \\ \text{s.t. } s_s = \{s_{s,1}, s_{s,2}, \ldots, s_{s,N_{fs}}\} \subset \Omega_s \\ \quad s_o = \{s_{o,1}, s_{o,2}, \ldots, s_{o,N_{fo}}\} \subset \Omega_{is} \end{cases} \tag{19}$$

In (19), N_{fo} is fixed and N_{fs} is gradually increased to meet the objective function. The optimization iteration is stopped when the rank of $\boldsymbol{T}_p$ does not grow with the increase of N_{fs}. The optimized N_{fs} is derived from the last iteration. It is necessary to mention that the original variation range of the pre-

served parameter has been segmented into k_{ps} parameter subspaces at Stage 1. Thus, the optimizing frequency interpolation process should be executed in each parameter subspace.

3) Stage 3: Constructing Projection Matrix

Based on the optimized parameter and frequency interpolation strategies, the proposed FDA-PMOR method constructs the projection matrix $\boldsymbol{T}_{p,k}$ for each parameter subspace using (7) and (11), as shown in Fig. 5 [33].

4) Stage 4: Building PROIM of MCFS

At Stage 4, the PROIM $Z_r(s,\lambda)$ consisting of $Z_{r,k}(s,\lambda)$ can be built individually by (5) and (6) at each parameter subspace as:

$$Z_r(s,\lambda)=\begin{cases} Z_{r,1}(s,\lambda) & \lambda\in\mathbb{S}_1 \\ Z_{r,2}(s,\lambda) & \lambda\in\mathbb{S}_2 \\ \vdots & \\ Z_{r,k}(s,\lambda) & \lambda\in\mathbb{S}_k \end{cases} \tag{20}$$

IV. Simulation Verification and Discussion

In this section, the proposed FDA-PMOR method is evaluated using three different scales of MCFSs.

A. Small-scale MCFS with Four Paralleled CREGs

The PROIM of the small-scale MCFS is built using the proposed FDA-PMOR method and three other methods, i.e., SLRCF-ADI-BT, traditional KS-PMOR, and partially-improved KS-PMOR methods. The output current I_{d0} of MCFS at steady-state setpoints is taken as the preserved parameter during the model order reduction.

Among these three benchmark methods, the SLRCF-ADI-BT method is initially proposed to build the parametric reduced-order model of large-scale power systems [23], [24]. The traditional KS-PMOR method obtains the PROIM without interpolation optimization [25], [31]. The partially-improved KS-PMOR method is designed to validate the necessity of the interpolation optimization, where only the parameter interpolation strategy is optimized. The FIPs are 2000 uniformly distributed frequency points within $\Omega=[0, 2000]$ Hz. The errors of PROIM obtained by different methods are shown in Fig. 7.

As shown in Fig. 7(a) and (b), by utilizing the SLRCF-ADI-BT method, the obtained PROIM of MCFS has relatively larger magnitude and phase errors. This is because the preserved parameters (I_{d0} of CREG in this case) are usually located in each CREG of MCFS. It is difficult to properly segment the full-order model of MCFS into the parameter-dependent decoupled internal system and the parameter-independent external system, which is quite different from the case of large-scale power systems in [27].

In Fig. 7(c)-(f), the errors of PROIM obtained by traditional KS-PMOR and partially-improved KS-PMOR methods are mostly concentrated in the I_{d0}-dominated low-frequency band. These errors are mainly caused by improper parameter and frequency interpolation. However, the magnitude and phase errors of the proposed FDA-PMOR method shown in Fig. 7(g) and (h) can be kept within 0.1 dB and 1.0°, respectively. Compared with the traditional KS-PMOR and the partially-improved KS-PMOR methods, the maximum magnitude errors with the proposed FDA-PMOR method are reduced by 97.35% and 80.39%, respectively, and the maximum phase errors are reduced by 79.26% and 47.12%, respectively. It indicates that parameter interpolation optimization and frequency interpolation optimization strategies are both important in building the high-precision PROIM of MCFS. Moreover, using the proposed FDA-PMOR method, the size of the obtained PROIM can be reduced by 15 orders, i.e., about 46% lower than the original 28-order full-order impedance model.

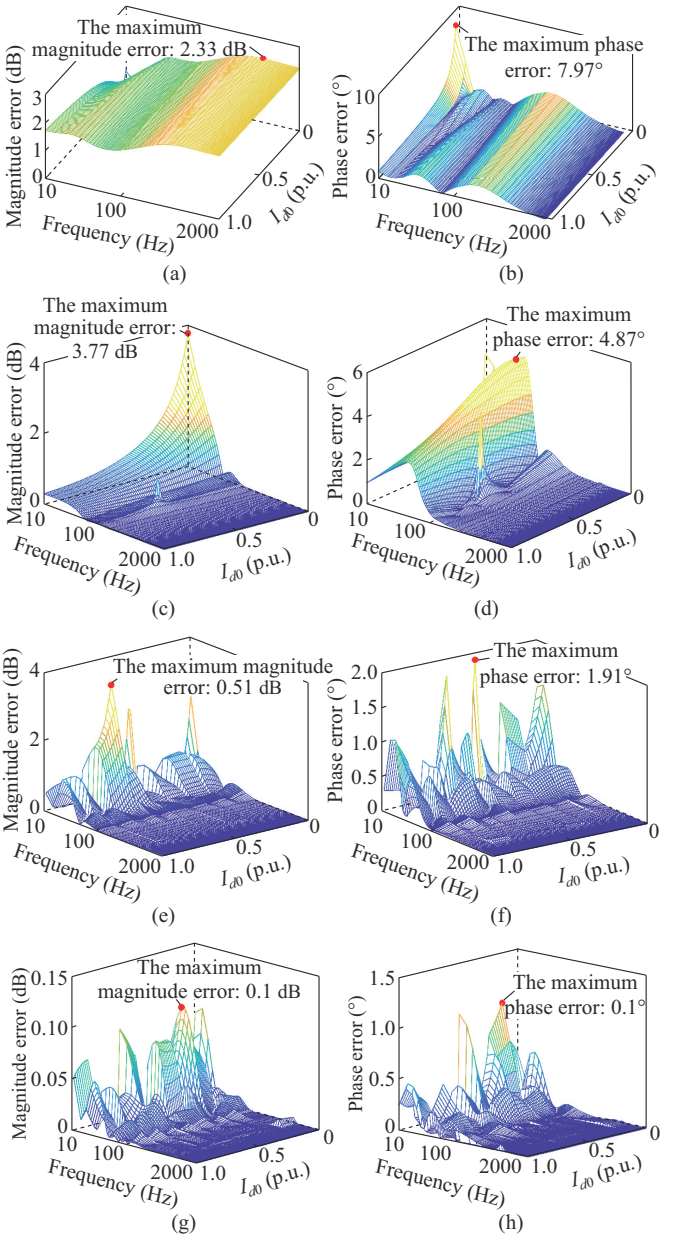

Fig. 7. Errors of PROIM obtained by different methods. (a) Magnitude error by SLRCF-ADI-BT method. (b) Phase error by SLRCF-ADI-BT method. (c) Magnitude error by traditional KS-PMOR method. (d) Phase error by traditional KS-PMOR method. (e) Magnitude error by partially-improved KS-PMOR method. (f) Phase error by partially-improved KS-PMOR method. (g) Magnitude error by proposed FDA-PMOR method. (h) Phase error by proposed FDA-PMOR method.

Comprehensively, the proposed FDA-PMOR method has a lower error than other three methods. The obtained PROIM

has a small size while maintaining a wide-band frequency-domain consistency over the full parameter range. These results do not affect the excellent performance of other methods when applied to other fields, such as the SLRCF-ADI-BT method in large-scale power systems [23].

B. Real-time Simulation-based MCFS with Eighteen Paralleled CREGs

In this subsection, the proposed FDA-PMOR method is validated using a 4.2 MW real-time simulation-based MCFS with eighteen paralleled CREGs. The specific parameters of each CREG in the large-scale MCFS are presented in Supplementary Material A Table SAII.

1) Error Evaluation of Obtained PROIM

In this case, the output current I_{d0} and the active damping factor K_c of each CREG at the steady-state setpoints are preserved. I_{d0} and K_c influence the impedance characteristics of MCFS at low- and high-frequency bands, respectively. By simultaneously preserving these two parameters, the efficacy of the proposed FDA-PMOR method in both low- and high-frequency bands can be validated.

According to the proposed FDA-PMOR method, the parameter space of I_{d0} and K_c has been divided into 10 parameter subspaces, and the obtained PROIM of MCFS consists of 10 different local PROIMs corresponding to each parameter subspaces. To comprehensively evaluate the errors of the obtained PROIM, 40 randomly generated and uniformly distributed K_c-I_{d0} combinations, as shown in Supplementary Material A Fig. SA1, are used as the test parameter sets. By substituting these test parameter sets into the obtained PROIM, the magnitude and phase errors of PROIM with different K_c-I_{d0} combinations are shown in Fig. 8, where the index of different K_c-I_{d0} combinations ranges from 1 to 40.

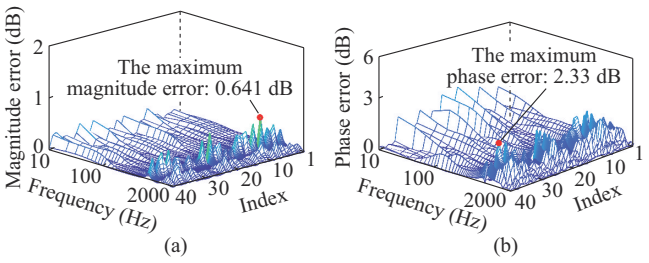

Fig. 8. Magnitude and phase errors of PROIM with different K_c-I_{d0} combinations. (a) Magnitude error. (b) Phase error.

It can be observed that most of the magnitude and phase errors can be kept within 0.5 dB and 2°, respectively. These results indicate that the proposed FDA-PMOR method has a superior wide-band accuracy performance when low- and high-frequency characteristics are preserved simultaneously. Moreover, with the proposed FDA-PMOR method, the model size of each local PROIM can be controlled around 26 orders, which is 81.9% less than the 144-order full-order impedance model. Compared with the small-scale MCFS with four paralleled CREGs, the model size of this large-scale MCFS can be reduced more significantly by the proposed FDA-PMOR method. Thus, the proposed FDA-PMOR method is better suited for model order reduction of large-scale MCFS. This viewpoint will be further validated on a larger MCFS with ninety paralleled CREGs in Section IV-C.

2) Application of Obtained PROIM to Oscillatory Stability Analysis

The real-time simulation platform for MCFS with eighteen paralleled CREGs is established based on the real-time digital simulation system (RTDS), as shown in Supplementary Material A Fig. SA2.

To verify the validation of the obtained PROIM in the wide-band oscillatory stability analysis, two typical scenarios of MCFS with sub-synchronous oscillation and high-frequency oscillation are used. The oscillatory stability is analyzed by performing the Nyquist criterion on the impedance return ratio $L(s)$:

$$L(s)=\frac{Z_{\mathrm{eg}}(s)}{Z_{\mathrm{MCFS}}(s)} \tag{21}$$

1) Scenario 1: sub-synchronous oscillation

The sub-synchronous oscillations, caused by the negative impedance interaction of MCFS and the grid in the low-frequency band, are the most frequent oscillations in a real MCFS. In this scenario, the MCFS is tied to a weak grid ($SCR=0.815$), the specific parameters of which are given in Supplementary Material A Table SAII, and the sub-synchronous oscillations may be triggered when the output power of MCFS fluctuates.

In this study, the normalized output power data from a practical wind turbine based MCFS are fed into the obtained PROIM as I_{d0} to simulate the continued varying operation point of the actual MCFS. The output wind power data set contains data of two days with a resolution of 5 min (with 576 data points included), as shown in Fig. 9(a).

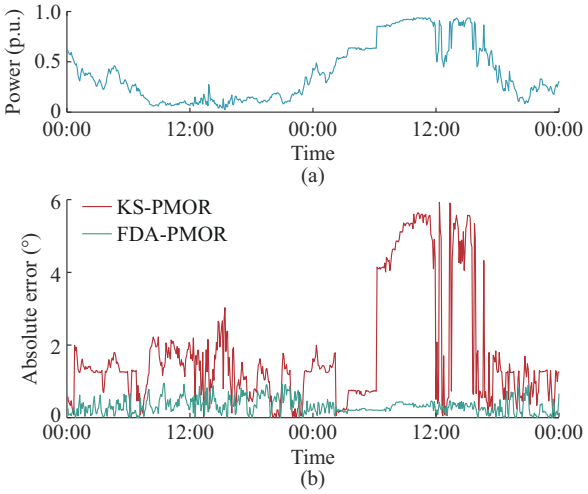

Fig. 9. Output wind power and absolute error of phase margin. (a) Output wind power. (b) Absolute error.

The accuracy of oscillatory stability analysis is evaluated by the phase margin of $L(s)$. The absolute errors of the phase margin obtained by the traditional KS-PMOR method and the proposed FDA-PMOR method are compared in Fig. 9(b). The absolute error of phase margin obtained by the traditional KS-PMOR method is higher than that by the proposed FDA-PMOR method over the full power range. Using the

proposed FDA-PMOR method, the absolute error of phase margin can be kept within 1°, which is sufficient to accurately predict the oscillatory risk of MCFS.

The computational burden of the oscillatory stability analysis is evaluated using a personal computer with 2.6 GHz Intel Core-i7 CPU and 16 GB RAM in the MATLAB environment. The comparison of execution time and memory usage for the oscillatory stability analysis with the full-order impedance model and the obtained PROIM are shown in Table II.

TABLE II
COMPARISON OF EXECUTION TIME AND MEMORY USAGE FOR OSCILLATORY STABILITY ANALYSIS WITH FULL-ORDER IMPEDANCE MODEL AND OBTAINED PROIM

Model	Execution time (s)	Memory usage (KB)
Full-order model	216.804	3220
PROIM	48.815	108

Using the obtained PROIM, the time consumption of the oscillatory stability analysis across all 576 data points can be reduced by 77.48% (the speedup factor is about 4.44), while the total memory usage can be reduced by 96.65%. This indicates the advantages of PROIM when used for oscillatory stability analysis of the large-scale MCFS.

To further evaluate if the obtained PROIM can correctly access the dominated oscillation modes in terms of oscillation frequencies and stability margins, one critical instability case with the power fluctuation is presented and analyzed.

In this case, the output power of MCFS, i.e., the value of I_{d0}, increases from 0.76 p.u. to 0.81 p.u.. During the oscillatory stability analysis, the full-order impedance model and the PROIMs obtained by different model order reduction methods are substituted into (21). The Nyquist diagram of impendance return ratios with different I_{d0} is shown in Fig. 10.

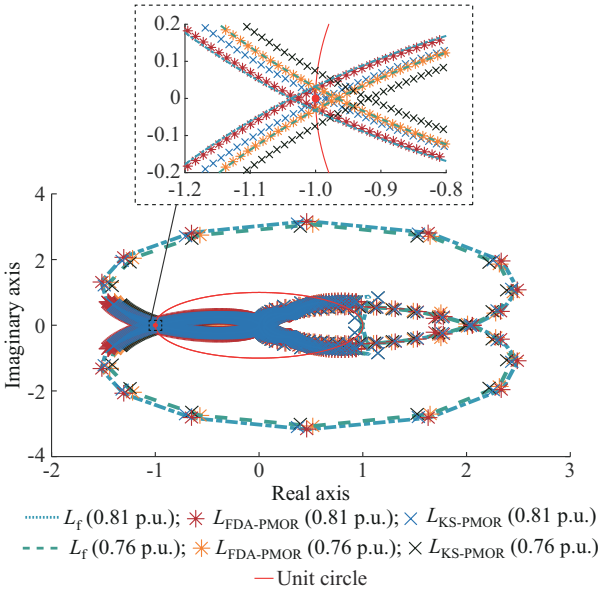

Fig. 10. Nyquist diagram of impedance return ratios with different I_{d0}.

In Fig. 10, the Nyquist curve of L_f encircles the point $(-1,0)$ when $I_{d0}=0.81$ p.u., which means that the system enters the unstable region. From the interaction point of the Nyquist curve and the unit circle, the phase margins and the oscillation frequencies can be obtained, as shown in Table III.

TABLE III
PHASE MARGINS AND OSCILLATION FREQUENCIES IN SCENARIO 1

Impedance return ratio	Phase margin (°)		Oscillation frequency (Hz)	
	$I_{d0}=0.76$ p.u.	$I_{d0}=0.81$ p.u.	$I_{d0}=0.76$ p.u.	$I_{d0}=0.81$ p.u.
L_f	1.72	–1.92		23.5
$L_{KS\text{-}PMOR}$	4.14	0.54		27.2
$L_{FDA\text{-}PMOR}$	1.66	–1.51		24.0

It can be inferred that using L_f and $L_{FDA\text{-}PMOR}$ has similar stability analysis results, and the theoretical oscillation frequencies are 23.5 Hz and 24 Hz in the *dq*-domain, respectively. However, the stability evaluation result of MCFS is incorrect using $L_{KS\text{-}PMOR}$.

The real-time simulation results with low-frequency oscillation are presented in Fig. 11. It can be found that the active power output P and the three-phase output currents I_a, I_b, and I_c measured at the PCC of MCFS suffer from subsynchronous oscillations after the power increase. The fast Fourier transform (FFT) analysis of I_a shows that the oscillation frequencies are 27 Hz and 73 Hz, corresponding to 23 Hz in the *dq*-domain. This result is close to the theoretical analysis using $L_{FDA\text{-}PMOR}$ and L_f.

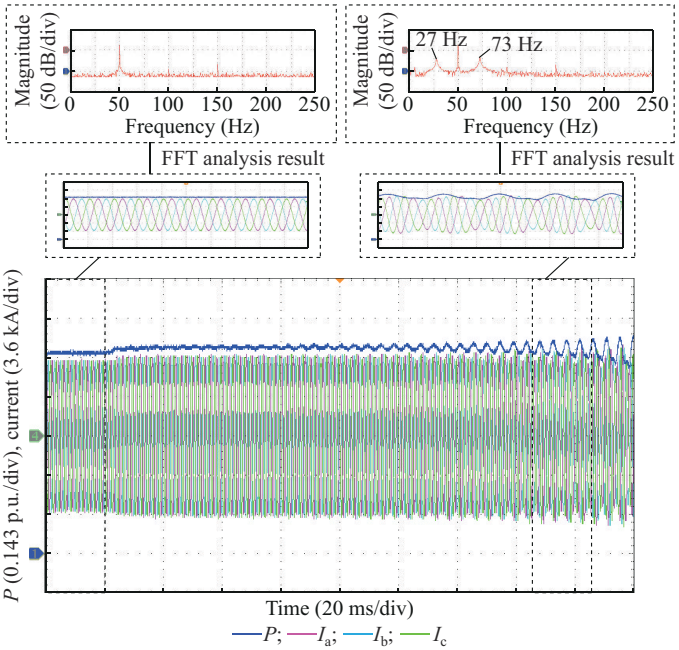

Fig. 11. Real-time simulation results with low-frequency oscillation.

2) Scenario 2: high-frequency oscillation

Another typical type of oscillations of MCFS is high-frequency oscillation. In this scenario, supposing that the active damping factor K_c of the current controller is not well tuned in some CREGs, the resonance peaks of the current controller and the output filter cannot be well damped. The grid im-

pedance coincidentally interacts with the MCFS impedance in the undamped frequency band, and the high-frequency oscillations are triggered.

Since the PROIM used in this scenario is the same as that in scenario 1, the evaluation of computational burden for the oscillatory stability analysis is not repeated. A typical high-frequency oscillation case is presented to verify the efficacy of PROIM for the oscillatory stability analysis in high-frequency band. In this case, the active damping factor K_c changes from 0 to 0.3, and the same analysis as in scenario 1 is conducted. Due to page limitations, the specific analyses are omitted here, only some essential analysis and test results are presented, as shown in Fig. 12, Table IV, and Fig. 13.

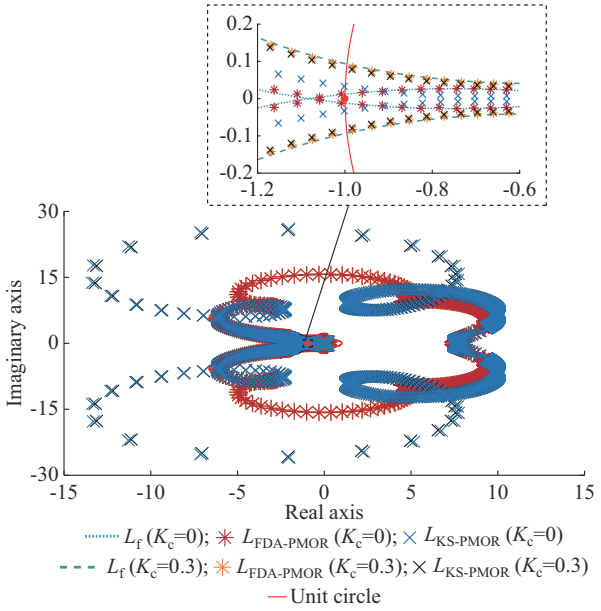

Fig. 12. Nyquist diagram of impedance return ratio with different K_c.

TABLE IV
PHASE MARGINS AND OSCILLATION FREQUENCIES IN SCENARIO 2

Impedance return ratio	Phase margin (°)		Oscillation frequency (Hz)	
	K_c=0	K_c=0.3	K_c=0	K_c=0.3
L_f	–0.69	5.23	1010	
$L_{KS-PMOR}$	1.79	4.50	1019	
$L_{FDA-PMOR}$	–0.91	4.87	1012	

These results indicate that compared with the traditional KS-PMOR method, the PROIM obtained by the proposed FDA-PMOR method also has higher accuracy for oscillatory stability analysis in the high-frequency band.

According to the above analysis of two typical scenarios, the PROIM obtained by the proposed FDA-PMOR method can significantly reduce the computational burden of oscillatory stability analysis. Meanwhile, the accuracy of oscillatory stability analysis can be maintained in terms of stability margins and oscillation frequencies, regardless of whether the dominant oscillation mode is in the low- or high-frequency band.

C. Larger MCFS with Ninety Paralleled CREGs

To further validate the applicability of the proposed FDA-PMOR method for larger MCFS in terms of accuracy and speedup, a case of 21 MW MCFS with ninety paralleled CREGs is analyzed in this subsection. The detailed parameters of MCFS and the parameter settings for the model order reduction are identical to the case in Section IV-B, except that the numbers of each type of CREG in MCFS are increased from 6 to 30.

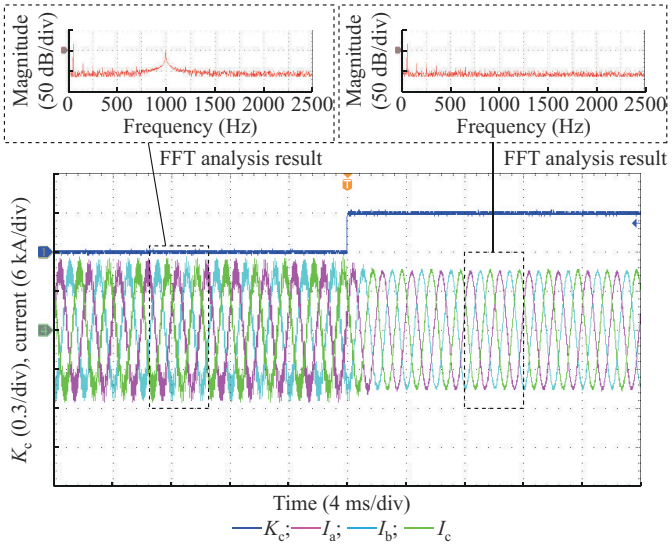

Fig. 13. Real-time simulation results with high-frequency oscillation.

The detailed simulation results are presented in Supplementary Material A. From the magnitude and phase error diagrams for PROIM in Supplementary Material A Fig. SA3, it can be observed that most of the amplitude and phase errors can be kept within 0.7 dB and 3°, respectively. Meanwhile, the model size of the obtained PROIM can be maintained around 26 orders, which is only 3.6% of the 720-order full-order impedance model. Compared with the MCFS with eighteen CREGs, the accuracy and model size of the obtained PROIM of this larger MCFS show no substantial increase.

The PROIMs obtained via the traditional KS-PMOR method and the proposed FDA-PMOR method are next employed for oscillatory stability analysis. The absolute error of margin at different operation points is shown in Supplementary Material A Fig. SA4. It is presented that the phase margin error of the proposed FDA-PMOR method shows a noticeable decline to the traditional KS-PMOR method.

Moreover, in this larger MCFS, the speedup factor of the oscillatory stability analysis can be examined. It is improved to 29.31 by using the obtained PROIM, as shown in Supplementary Material A Table SAIII, which is about 6.6 times higher than the case in Section IV-B. The average execution time for one single stability analysis is about 0.088 s.

V. CONCLUSION

This paper proposes an FDA-PMOR method to reduce the computational burden of oscillatory stability analysis by

building precise PROIM of MCFS. The efficiency and practicability of the proposed FDA-PMOR method are validated by three MCFSs of different scales. The main conclusions are as follows.

1) The factors associated with the errors of model order reduction are estimated by defining three indicators, i.e., the convergence error, cumulative error, and rank of projection matrix. These are obtained by quantitively analyzing the error mechanism of the traditional KS-PMOR method.

2) The FDA-PMOR method is proposed to build the PROIMs of MCFSs. Different from the traditional KS-PMOR method, it can adaptively optimize the parameters and frequency interpolation strategies based on the three indicators. As a result, the accuracy of PROIM can be notably improved. Compared with the three other methods, i.e., SLR-CF-ADI-BT, traditional KS-PMOR, and partially-improved KS-PMOR methods, the maximum magnitude errors by the proposed FDA-PMOR method are reduced by 95.71%, 97.35%, and 80.39%, respectively, and the maximum phase errors are reduced by 87.33%, 79.26%, and 47.12%, respectively.

3) The obtained PROIM accelerates the oscillatory stability analysis of MCFSs with eighteen paralleled CREGs and ninety paralleled CREGs by 4.44 and 29.31 times, respectively, while the accuracy of oscillatory stability analysis is maintained in both stability margin and oscillation frequency. It is evident that, for larger MCFS with more CREGs, the proposed FDA-PMOR method not only preserves higher accuracy but also exhibits better model reduction performance.

According to the above discussions, the proposed FDA-PMOR method can be used for model order reduction to build precise PROIMs of MCFSs with large numbers of CREGs. The obtained PROIMs are promising for the real-time (or near real-time) oscillatory stability analysis of large-scale MCFS or regional power systems with clusters of large-scale MCFSs.

In future work, the advanced stability criterion will be further investigated in combination with the obtained PROIM for the real-time oscillatory stability analysis of MCFS cluster based regional power systems in different grid states, such as the unbalanced grid and the fundamental frequency fluctuation.

REFERENCES

[1] N. Hatziargyriou, J. Milanovic, C. Rahmann *et al*., "Definition and classification of power system stability – revisited & extended," *IEEE Transactions on Power Systems*, vol. 36, no. 4, pp. 3271-3281, Jul. 2021.

[2] J. Shair, X. Xie, J. Yang *et al*., "Adaptive damping control of subsynchronous oscillation in DFIG-based wind farms connected to series-compensated network," *IEEE Transactions on Power Delivery*, vol. 37, no. 2, pp. 1036-1049, Apr. 2022.

[3] G. He, W. Wang, and H. Wang, "Coordination control method for preventing sub/super synchronous oscillations of multi-wind farm systems," *CSEE Journal of Power and Energy Systems*, vol. 9, no. 5, pp. 1655-1665, Sept. 2023.

[4] X. Zhang, F. Zhang, W. Gao *et al*., "Improved subsynchronous oscillation parameter identification with synchrophasor based on matrix pencil method in power systems," *Journal of Modern Power Systems and Clean Energy*, vol. 12, no. 1, pp. 22-33, Jan. 2024.

[5] J. Shair, X. Xie, and G. Yan, "Mitigating subsynchronous control interaction in wind power systems: existing techniques and open challenges," *Renewable and Sustainable Energy Reviews*, vol. 108, pp. 330-346, Jul. 2019.

[6] W. Dong, W. Du, X. Xie *et al*., "An approximate aggregated impedance model of a grid-connected wind farm for the study of small-signal stability," *IEEE Transactions on Power Systems*, vol. 37, no. 5, pp. 3847-3861, Sept. 2022.

[7] J. Billo, A. B. Hansen, J. Leslie *et al*. Inaugural Research Agenda. Global Power System Transformation (G-PST) Consortium, Colombia, SC, Tech. Rep, 2022.

[8] X. Xu, R. M. Mathur, J. Jiang *et al*., "Modeling of generators and their controls in power system simulations using singular perturbations," *IEEE Transactions on Power Systems*, vol. 13, no. 1, pp. 109-114, Feb. 1998.

[9] U. Buragohain and N. Senroy, "Reduced order DFIG models for PLL-based grid synchronization stability assessment," *IEEE Transactions on Power Systems*, vol. 38, no. 5, pp. 4628-4639, Sept. 2023.

[10] P. Vorobev, P. H. Huang, M. A. Hosani *et al*., "High-fidelity model order reduction for microgrids stability assessment," *IEEE Transactions on Power Systems*, vol. 33, no. 1, pp. 874-887, Jan. 2018.

[11] M. Juneja, S. K. Nagar, and S. R. Mohanty, "ABC based reduced order modelling of microgrid in grid-tied mode," *Control Engineering Practice*, vol. 84, pp. 337-348, Mar. 2019.

[12] R. Wang, Q. Sun, P. Zhang *et al*., "Reduced-order transfer function model of the droop-controlled inverter via Jordan continued-fraction expansion," *IEEE Transactions on Energy Conversion*, vol. 35, no. 3, pp. 1585-1595, Sept. 2020.

[13] V. Purba, B. B. Johnson, M. Rodriguez *et al*., "Reduced-order aggregate model for parallel-connected single-phase inverters," *IEEE Transactions on Energy Conversion*, vol. 34, no. 2, pp. 824-837, Jun. 2019.

[14] N. Shabanikia and S. A. Khajehoddin, "Weighted dynamic aggregation modeling of grid-following inverters to analyze renewable DG integrated microgrids," *IEEE Transactions on Industrial Electronics*, vol. 71, no. 1, pp. 583-594, Jan. 2024.

[15] M. Y. Morgan, A. A. El-Deib, and M. El-Marsafawy, "Wind farm dynamic models assessment under weak grid conditions," *IET Renewable Power Generation*, vol. 12, no. 12, pp. 1325-1334, Sept. 2018.

[16] Y. Wu, J. Zeng, G. Lu *et al*., "Development of an equivalent wind-farm model for frequency regulation," in *Proceedings of 2019 IEEE Industry Applications Society Annual Meeting*, Baltimore, USA, Sept. 2019, pp. 1-12.

[17] B. Shao, S. Zhao, B. Gao *et al*., "Adequacy of the single-generator equivalent model for stability analysis in wind farms with VSC-HVDC systems," *IEEE Transactions on Energy Conversion*, vol. 36, no. 2, pp. 907-918, Jun. 2021.

[18] Q. Chen, S. Bu, and C. Y. Chung, "Small-signal stability criteria in power electronics-dominated power systems: a comparative review," *Journal of Modern Power Systems and Clean Energy*, vol. 12, no. 4, pp. 1003-1018, Jul. 2024.

[19] M. Zhang, X. Wang, D. Yang *et al*., "Artificial neural network based identification of multi-operating-point impedance model," *IEEE Transactions on Power Electronics*, vol. 36, no. 2, pp. 1231-1235, Feb. 2021.

[20] W. Du, B. Ren, H. Wang *et al*., "Comparison of methods to examine sub-synchronous oscillations caused by grid-connected wind turbine generators," *IEEE Transactions on Power Systems*, vol. 34, no. 6, pp. 4931-4943, Nov. 2019.

[21] H. R. Ali, L. P. Kunjumuhammed, B. C. Pal *et al*., "Model order reduction of wind farms: linear approach," *IEEE Transactions on Sustainable Energy*, vol. 10, no. 3, pp. 1194-1205, Jul. 2019.

[22] X. Jiang, M. Mao, and L. Chang, "Adaptive reduced-order method of aggregated impedance model for large-scale photovoltaic stations small signal stability analysis," in *Proceedings of 2022 IEEE Energy Conversion Congress and Exposition*, Detroit, USA, Oct. 2022, pp. 1-8.

[23] Y. G. I. Acle, F. D. Freitas, N. Martins *et al*., "Parameter preserving model order reduction of large sparse small-signal electromechanical stability power system models," *IEEE Transactions on Power Systems*, vol. 34, no. 4, pp. 2814-2824, Jul. 2019.

[24] F. D. Freitas, J. Rommes, and N. Martins, "Gramian-based reduction method applied to large sparse power system descriptor models," *IEEE Transactions on Power Systems*, vol. 23, no. 3, pp. 1258-1270, Aug. 2008.

[25] Z. Zhang, I. M. Elfadel, and L. Daniel, "Model order reduction of fully parameterized systems by recursive least square optimization," in *Proceedings of 2011 IEEE/ACM International Conference on Computer-aided Design*, San Jose, USA, Nov. 2011, pp. 523-530.

[26] P. Benner, S. Gugercin, and K. Willcox, "A survey of projection-based model reduction methods for parametric dynamical systems," *SIAM Review*, vol. 57, no. 4, pp. 483-531, Jan. 2015.
[27] U. Baur, C. Beattie, P. Benner *et al*., "Interpolatory projection methods for parameterized model reduction," *SIAM Journal on Scientific Computing*, vol. 33, no. 5, pp. 2489-2518, Jan. 2011.
[28] D. Zhu, S. Zhou, X. Zou *et al*., "Improved design of PLL controller for LCL-type grid-connected converter in weak grid," *IEEE Transactions on Power Electronics*, vol. 35, no. 5, pp. 4715-4727, May 2020.
[29] S. Liao, Y. Chen, W. Wu *et al*., "Closed-loop interconnected model of multi-inverter-paralleled system and its application to impact assessment of interactions on damping characteristics," *IEEE Transactions on Smart Grid*, vol. 14, no. 1, pp. 41-53, Jan. 2023.
[30] W. Wang, G. Li, and G. He, *Analysis and Mitigation of Broadband Oscillation in Renewable Energy Generation and AC/DC Transmission Systems*. Singapore: Springer, 2023.
[31] Y. Jiang, "Krylov subspace model order reduction methods," *in Model Order Reduction Method*. Beijing: Science Press, 2010.
[32] Golub, H. Gene, and C. F. V. Loan, *Matrix Computations*. Baltimore: Johns Hopkins University Press, 2013.
[33] Z. Zhu, G. Geng, and Q. Jiang, "Power system dynamic model reduction based on extended Krylov subspace method," *IEEE Transactions on Power Systems*, vol. 31, no. 6, pp. 4483-4494, Nov. 2016.

Xun Jiang received the B.Sc. degree in the School of Electrical Engineering from Anhui Polytechnic University, Wuhu, China, in 2017. He is currently working toward the Ph.D. degree at Hefei University of Technology (HFUT), Hefei, China. He is the Post Chair of IEEE Power Electronics Society Student Branch Chapter at HFUT. His research interest includes power electronic integrated power system stability analysis.

Meiqin Mao received the B.Sc., M.Sc. and Ph.D. degrees in electrical engineering from Hefei University of Technology (HFUT), Hefei, China, in 1983, 1988, and 2004, respectively. She is now a Professor with HFUT. She serves as an Associate Editor for IEEE Journal of Emerging and Selected Topics in Power Electronics. Her research interests include distributed power generation, microgrid, and power electronics applied in power system.

Liuchen Chang received the B.Sc. degree from Northern Jiaotong University, Beijing, China, in 1982, the M.Sc. degree from the China Academy of Railway Sciences, Beijing, China, in 1984, and the Ph.D. degree from Queen's University, Kingston, Canada, in 1991. He is a Professor Emeritus of electrical and computer engineering and NSERC Chair at the University of New Brunswick, New Brunswick, Canada. He is a Fellow of Canadian Academy of Engineering. His research interests include distributed power generation, renewable energy, variable speed drives, and electric vehicle traction system.

Bao Xie received the B.S. and Ph.D. degrees in electrical engineering from Chongqing University, Chongqing, China, in 2014 and 2024, respectively. He is now a Lecturer with Hefei University of Technology (HFUT), Hefei, China. His research interests include renewable energy generation technology and control and stability of power converters.

Haijiao Wang received the B.Sc. and Ph.D. degrees from the Department of Electrical Engineering, Zhejiang University, Hangzhou, China, in 2009 and 2014, respectively. He is currently a Senior Engineer with the China Electric Power Research Institute, Beijing, China. His current research interests include the stability analysis and control for power system with large-scale renewable generation.

Nikos D. Hatziargyriou received the B.Sc. degree from National Technical University of Athens (NTUA), Athens, Greece, in 1976, the M.Sc. and Ph.D. degrees from The University of Manchester, Manchester, UK, in 1979 and 1982, respectively. He is a Professor Emeritus in power systems at the NTUA. He is Life Fellow of IEEE. His research interests include smart grid, microgrid, distributed and renewable energy source, and power system security.